Quadrupole and hexadecapole moments of ^{232}Th and ^{238}U from inelastic scattering of 65 MeV polarized protons

Y. Takeuchi, H. Sakaguchi, M. Nakamura, T. Ichihara,* M. Yosoi, M. Ieiri, and S. Kobayashi
Department of Physics, Kyoto University, Kyoto 606, Japan
(Received 25 April 1986)

Differential cross sections and analyzing powers of elastic and inelastic scattering of polarized protons from actinide nuclei (^{232}Th and ^{238}U) have been measured for the first time. A coupled-channel analysis has been performed for $J^{\pi}=0^{+}-6^{+}$ members of the ground state rotational band. Excellent fits have been obtained up to the 6^{+} state. Extracted quadrupole moments of the deformed optical potential are 1.0—2.0 % larger than those of the charge distribution. This difference is significantly small, compared with the case of the previous rare-earth region nuclei at 65 MeV (4—5 %). A realistic folding calculation based on the density- and energy-dependent effective interaction was performed. The effect of the Coulomb potential through the energy dependence of the effective interaction was found to be important to reproduce quadrupole moments of the deformed optical potential, especially for the actinide nuclei. Extracted hexadecapole moments are 14—18 % larger than those of the charge densities, and the possible sources of this difference in the hexadecapole moments will be discussed.

I. INTRODUCTION

The studies of the elastic and inelastic scattering of protons from permanently deformed nuclei have shed light on the understanding of the reaction mechanism as well as the nuclear structure.[1-8] In particular, the deformed optical potential (DOP) obtained from the coupled-channel analysis for the members of the ground state rotational band has been found to provide important information on the many-body properties of the proton-nucleus interaction. In the study of the proton optical potential, comparisons between the microscopic theory and the experiment have been made in terms of volume integrals and mean square radii of the optical potentials.[9] In the case of deformed optical potential, multipole moments are available as new physical quantities associated with the deformation of the mean field, in addition to the volume integrals and the mean square radii.

According to Satchler's theorem,[10] the multipole moments of the DOP should be equal to those of underlying matter density in the limit where the DOP is derived by folding the local and density independent interaction.[11-14] Therefore, the difference of the multipole moments between the DOP and the matter distribution should be explained by the many-body effects which are not included in the simple folding procedure. The multipole moments of the matter distribution are usually assumed to be equal to the multipole moments of the charge distribution. By comparing the multipole moments of the DOP with the electric multipole moments, we can obtain precise information on some many-body effects which are of much theoretical interest such as the density dependence of the effective interaction, independent of the range of the effective interaction. In our previous work on Er and Yb isotopes[2] at 65 MeV, we have found that the quadrupole moment of the real central part of the deformed optical potential is systematically 4—6 % larger than the electric quadrupole moment obtained by electron scattering and/or Coulomb excitation. We have shown that the difference is successfully explained by the effect of the density dependence of the effective interaction, assuming that the quadrupole moment of the charge density is equal to that of the neutron density. In the recent work on Hf and W isotopes,[3] precise measurements of the higher excited states up to 6^{+} made it possible to extend our method to the imaginary part and the spin-orbit part of the DOP. The multipole moments of the spin-orbit part have been found to be almost equal to those of the charge density as expected by the microscopic theory.[15]

Considering the above feature of the multipole moments of the DOP, further investigation of the multipole moments in other regions of deformed nuclei will reveal different many-body features of the proton-nucleus interaction. One of the prospective ways is to measure the inelastic scattering from actinide nuclei, which have much larger A, Z, and $N-Z$ values than rare earth nuclei. In the region of actinide nuclei, there were the pioneering works by the Michigan State University (MSU) group using 35 MeV unpolarized protons.[4,5]

We have extended the measurements of the differential cross sections and analyzing powers of the elastic and inelastic scattering of polarized protons to the actinide region. The experiment was performed for ^{232}Th and ^{238}U at 65 MeV. The advantages of the proton energy of 65 MeV and the use of a polarized beam have already been reported in our previous papers.[1-3,9] First, at this energy the influence of a giant resonance on the excitation of a low-lying collective state is small and the reaction mechanism is simple. Second, the DOP parameters can be determined with less ambiguities using analyzing power

data together with the cross sections. In addition, the use of a polarized beam offers us a reliable peak-fitting method in the data reduction, the details of which are presented in Sec. III.

In this paper we have described the experimental procedure in Sec. II. In Sec. III a new peak-fitting method devised for this work is presented. The coupled-channel analysis and the discussion about the uncertainties associated with the analysis are presented in Sec. III. In Sec. IV a comparison of the multipole moments of the DOP with those of charge densities and discussions based on the folding model calculation using a realistic effective interaction are presented. A summary and conclusions are given in Sec. V.

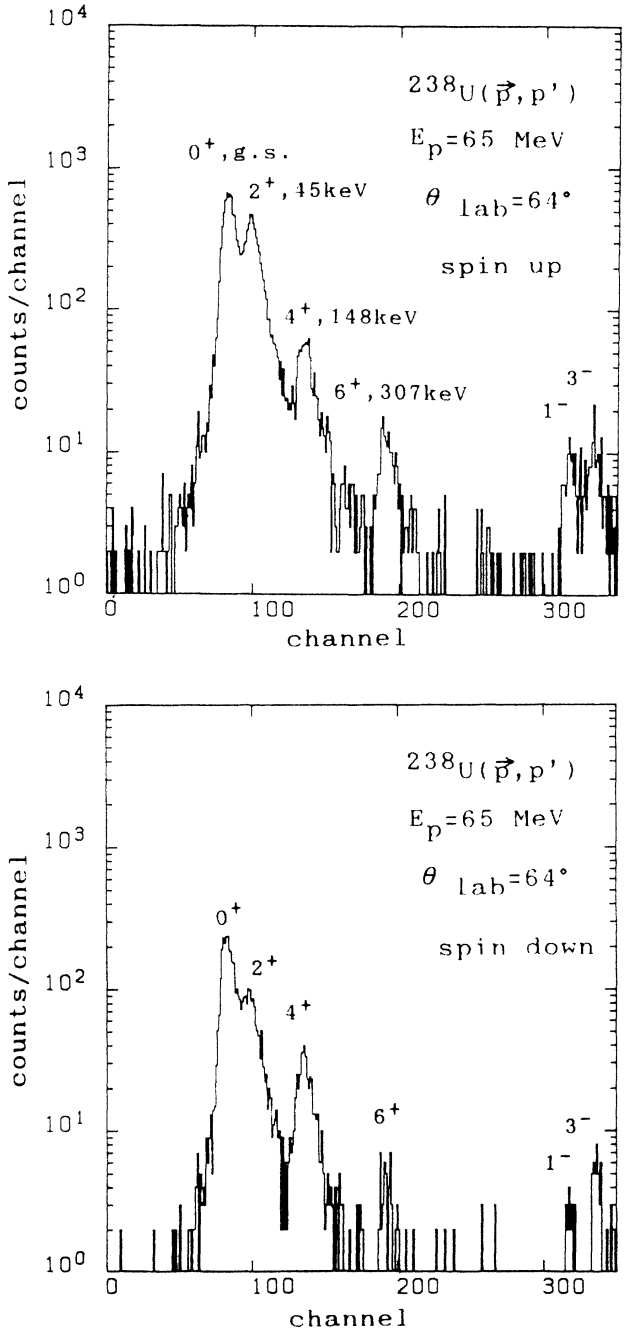

FIG. 1. Typical position spectra of the focal plane counter for the ^{238}U(p,p') scattering at 65 MeV. Spin-up and spin-down spectra are shown at $\theta_{lab}=64°$.

II. EXPERIMENTAL PROCEDURE

The experiment was carried out using a polarized proton beam of 65 MeV from the cyclotron at the Research Center for Nuclear Physics, Osaka University, and the data were obtained using a high resolution spectrograph RAIDEN.[16] The details of the polarized ion source and the beam transport system are presented in our previous papers.[2,17]

The beam polarization was monitored by a sampling type polarimeter.[18] Since the polarimeter is located upstream of the scattering chamber, the target of the polarimeter in the beam line deteriorated the quality of the beam considerably. Therefore, this type of polarimeter is indispensable for the high resolution measurements. A polyethylene target of the polarimeter was periodically inserted in the beam line for a few seconds to measure the beam polarization with a fixed interval of 10—50 sec, depending on the experimental condition. During the measurement of the beam polarization, the measurement of the momentum spectra was inhibited. The beam polarization was about 80%. The direction of the beam polarization was reversed every 0.5 sec to reduce the instrumental asymmetry. Typical beam intensity was 40 nA on target.

The targets used were in the form of natural uranium and thorium dioxides with nickel backings. They were prepared by electrodeposition from aqueous solutions of their sulfates.[19] By comparing the yields of the elastic scattering from ^{16}O, the absolute target thickness was determined with the cross section data of ^{16}O at 65 MeV,[9] provided that the chemical forms of the uranium (thorium) was pure UO_2 (ThO_2). The net uranium (thorium) content in the target was 0.72 (0.60) mg/cm^2. The thickness of backing nickel foil was 80 μg/cm^2. At the very forward angles where elastic peaks from nickel backing cannot be separated kinematically, aluminum backing targets prepared by electrodeposition from organic solutions[20] were used, whose thicknesses were limited by the properties of the backing material and were only 0.10 mg/cm^2 for ^{232}Th and 0.20 mg/cm^2 for ^{238}U, respectively.

The solid angles and angular acceptances of the spectrograph were 1.4 msr and $\pm 0.48°$ for the measurements at forward angles ($<42°$) and 2.5 msr and $\pm 0.72°$ at backward angles ($\geqq 42°$), respectively. The angular distributions were measured from 11° to 70° in 1.0° steps at the forward angles and 2.0° steps at the backward angles.

At the focal plane of the spectrograph, protons were detected by a counter array consisting of a two-dimensional position sensitive proportional counter of 1.5 m length, a pair of single wire proportional counters, and a plastic scintillator.[21] An event signal was generated by an energy signal from the plastic scintillator. At each event, the signals from the counter system were digitized by analog-to-digital converters (ADC's) and transferred to the PDP-11/44 computer. All data were recorded on magnetic tapes in a list mode.

III. DATA REDUCTION AND ANALYSIS

A. Peak-fitting procedure

The momentum spectra were constructed from the list mode raw data by selecting events which have a complete set of the signals from the counter array. A typical momentum spectra for ^{238}U at $\theta_{lab}=64°$ are shown in Fig. 1. In the case of the ^{238}U target, the overall energy resolution was 20–22 keV full width at half maximum (FWHM) at the forward angles and 24–26 keV FWHM at the backward angles, respectively. However, as we notice from Fig. 1, the peak-to-valley ratio between the 0^+ and 2^+ states was considerably reduced due to the overlap of the tails of the peaks. When the elastic peak was dominant, a serious problem was caused to separate the 2^+ state whose excitation energy is less than 50 keV. Thus, we need a suitable peak-fitting procedure. In our previous works,[1–3] the peak shape was assumed to be identical to a certain reference function. This reference function was made by the well separated elastic peak of neighboring spherical nucleus such as ^{148}Sm. However, the peak shape varies with the condition of the beam transport system. The deviation of the reference function from the true peak shape caused considerable errors in the resultant peak counts for the 2^+ peak of the actinide nuclei. Our previous method is no longer suitable in this case. Thus, we had to improve our peak-fitting method.

In the present case, we modified the peak-fitting method by Blok *et al.*[22] with asymmetric shape in which the double exponentials are superposed on the Gaussian tails instead of smooth joining. We have assumed common shape for the peaks of the members of the ground state rotational band. Six parameters were used to adjust the peak shape. In addition, each peak has two parameters of the peak height and the peak position. These parameters are searched in each peak fitting. Most of the improvement in the description of the peak shape comes

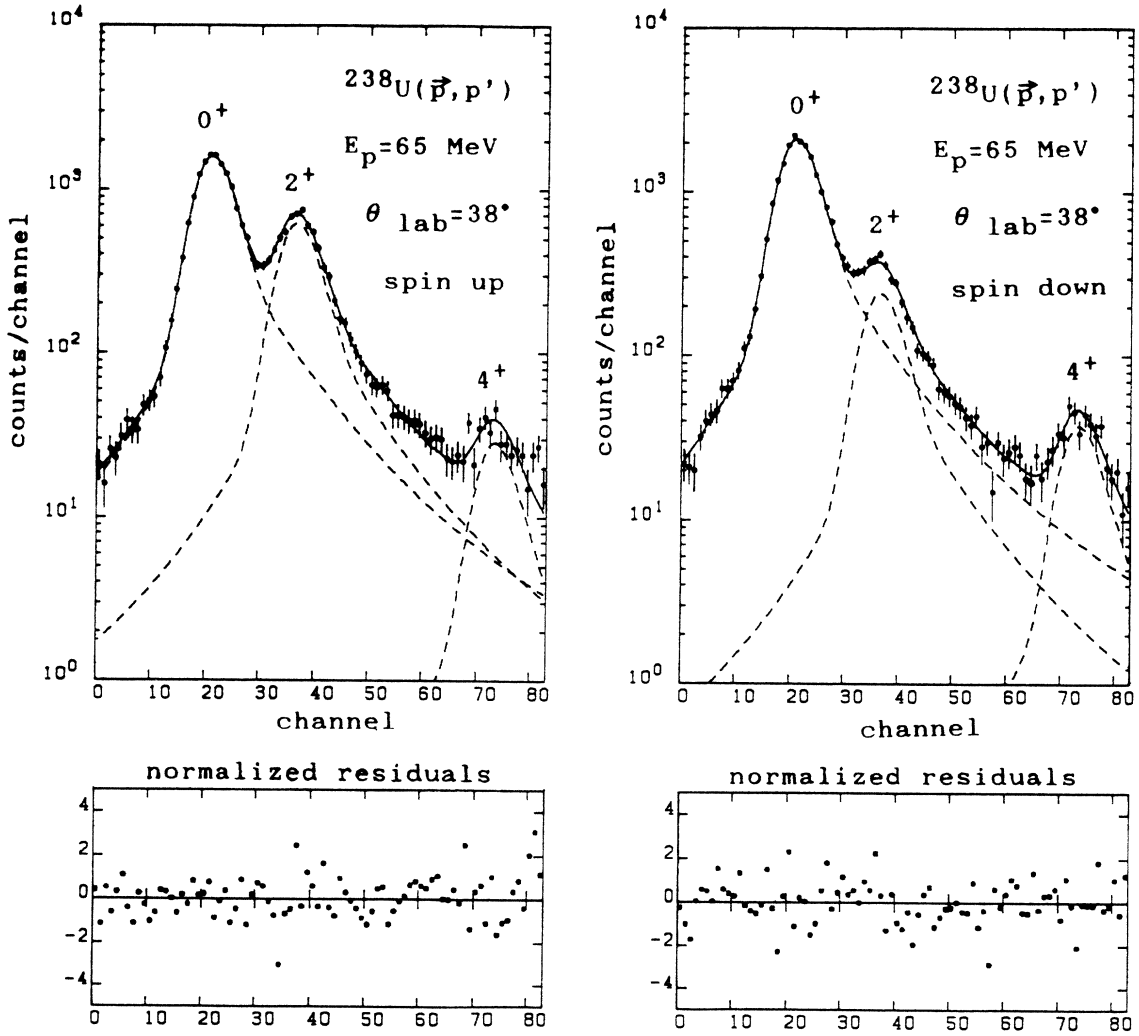

FIG. 2. Typical result of the peak fitting for the ^{238}U(p,p') scattering. The results of the spin-up and the spin-down spectra are shown at $\theta_{lab}=38°$. The solid circles represent the number of counts in each channel. The solid lines represent the results of the peak fitting procedure described in the text. The dashed curves represent calculated peaks corresponding to each state of ^{238}U. Normalized residuals, $s_i=(y_i-f_i)/\Delta y_i$, are also plotted, where y_i is the number of counts in ith channel, f_i are the calculated counts, and Δy_i is the standard deviation of y_i.

from the adoption of the double exponential shape for the tail of the peak.

In order to reduce the uncertainties in the search for the peak shape, the spectra of both spin modes were fitted simultaneously under the constraint that the peak shape and the peak positions of the spin-up spectrum should be equal to those of the spin-down spectrum in the same data-taking run. The rapid reversal of the direction of the beam polarization ensures this constraint. Since the analyzing powers of elastic and inelastic scattering are, in general, different at a given scattering angle, the spectra of both modes are different and complementary. Thus, the ambiguities were considerably reduced in most cases. Using the known spacing between the elastic and inelastic peaks, this procedure was applicable even for the cases where the 2^+ peaks of both spin modes were much smaller than the elastic peaks. At the very forward angles, peaks from the backing materials and the target contamination were also included in the fittings, but their peak shapes were searched independently in order to take account of the kinematical effects.

An example of the peak fitting is shown in Fig. 2. The χ^2 values per data point were 1.0–1.5 for both spin modes. The normalized residuals are also shown in the same figure, and we notice that systematic deviations can hardly be observed. The resultant values of the peak shape parameters showed stable behaviors, corresponding to the experimental conditions. These results ensure the reliability of the peak shape function. This new peak-fitting procedure was also tested in the spectra of our previous rare earth nuclei. The resultant counts in peak area agreed well with those from the old procedure. Therefore, the new method is thought to have more general applicability than the previous one.

The uncertainties of the peak sums were calculated with the use of the error matrix of the searched parameters in the fitting. Therefore, these uncertainties also contain the ambiguities of the peak shape. The experimental cross sections and analyzing powers are plotted in Figs. 3 and 4. The long error bars at the forward angles of the 2^+ states are due to the uncertainties from the peak-sum extraction. At the forward angles, the dominance of the elastic peak over the peak of the 2^+ state and the inclusion of the peaks from the contamination in the target made peak separation of the 2^+ state difficult in the fitting.

B. Analysis

Coupled-channel analysis has been performed for the $J^\pi=0^+-6^+$ states of the ground state rotational band using the automatic search code ECIS79 of Raynal.[23,24] It was assumed that these states were members of a $K^\pi=0^+$ rotational band of the axially symmetric rigid rotor. In this analysis, the following deformed optical potential was used:

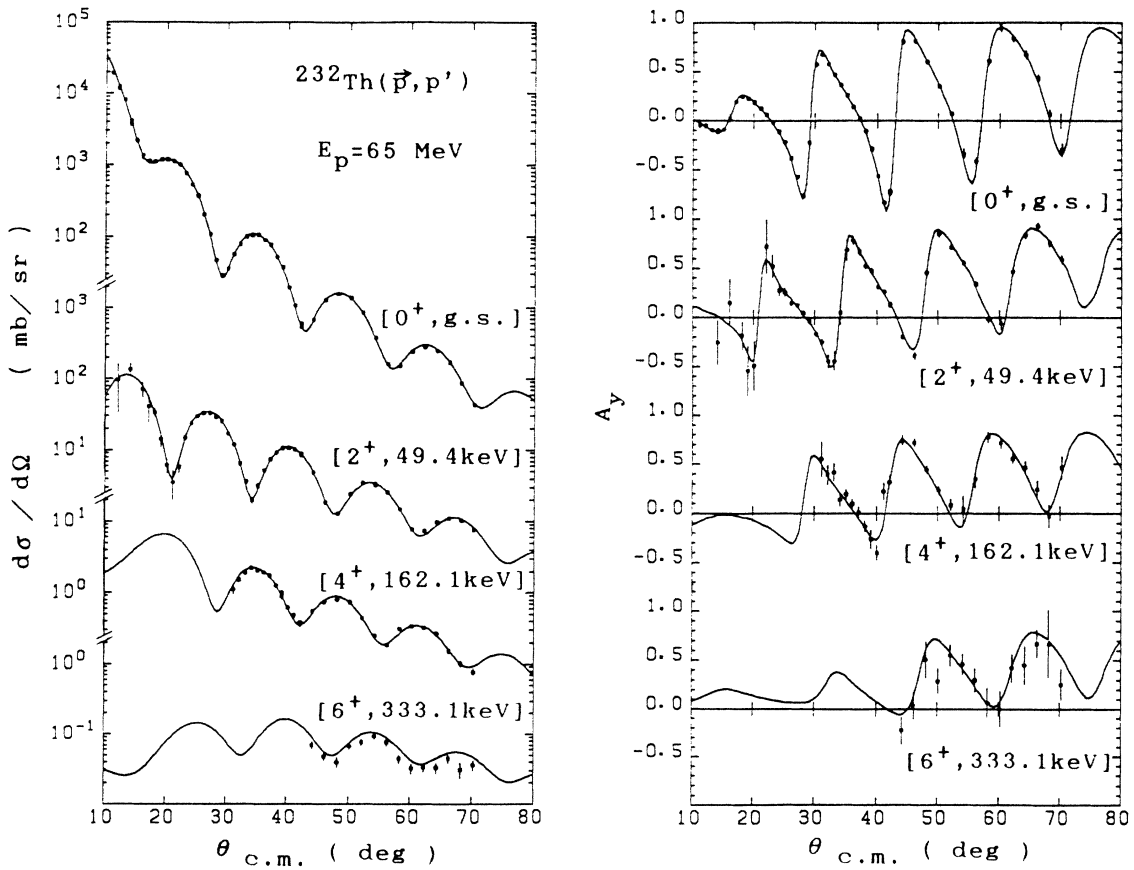

FIG. 3. Measured cross section and analyzing power for the ^{232}Th(p,p') scattering at 65 MeV. The error bars on the experimental data were calculated with the use of error matrix of the searched parameters in the peak fitting. The solid curves are results of the coupled-channel analysis. The DOP parameters are listed in Table I.

$$U(r,\theta)= V_{\mathrm{Coul}}(r;r_c(\theta),a_c)-V_R f(r;r_R(\theta),a_R)-iW_{wv}f(r;r_{wv}(\theta),a_{wv})+4ia_{ws}W_{ws}\frac{d}{dr}f(r;r_{ws}(\theta),a_{ws})$$
$$+V_{ls}\left[\frac{\hbar}{m_\pi c}\right]^2\frac{1}{r}\frac{d}{dr}f(r;r_{ls}(\theta),a_{ls})(\boldsymbol{\sigma}\cdot\mathbf{L})\ , \tag{1}$$

where

$$f(r;r_j(\theta),a_j)=(1+\exp\{[r-r_j(\theta)A^{1/3}]/a_j\})^{-1}\ , \tag{2}$$

and

$$r_j(\theta)=r_0^j\left[1+\sum_\lambda \beta_\lambda^j Y_{\lambda 0}(\theta)\right]\ . \tag{3}$$

The suffix j represents each part of the optical potential: the real central part (R), the volume imaginary part (wv), the surface imaginary part (ws), the spin-orbit part (ls), and the Coulomb part (c). Deformation parameters β_2, β_4, and β_6 were used. The spin-orbit part was the deformed full Thomas type. The Coulomb potential was assumed to arise from a deformed Fermi charge distribution and its geometrical parameters (the reduced radius, the diffuseness, and the deformation parameters) are fixed to the values of the electron scattering data at the Massachusetts Institute of Technology (MIT) Bates Linear Accelerator.[25,26] They are $r_c=1.09$ fm, $a_c=0.59$ fm, $\beta_2=0.273$, $\beta_4=0.073$, and $\beta_6=0.006$ for ^{238}U, and $r_c=1.10$ fm, $a_c=0.60$ fm, $\beta_2=0.243$, $\beta_4=0.090$, and $\beta_6=0.011$ for ^{232}Th, respectively.

The optical potential parameters and the deformation parameters were adjusted so as to optimize the fit to the angular distributions of the cross section and the analyzing power of the 0^+, 2^+, 4^+, and 6^+ states. In the process of the search for the DOP parameters, 3% errors were added to the statistical uncertainties in quadrature to include the unknown systematic error and to avoid trapping in an unphysical local χ^2 minimum as shown in the following forms:

$$\delta\left[\frac{d\sigma}{d\Omega}\right]=\left[\delta\left[\frac{d\sigma}{d\Omega}\right]^2_{\mathrm{stat}}+\left[\frac{d\sigma}{d\Omega}\right]^2\times 0.03^2\right]^{1/2}\ ,$$
$$\delta A_y=(\delta A_{y_{\mathrm{stat}}}^2+0.03^2)^{1/2}\ , \tag{4}$$

Considering the uncertainty in the target thickness estimation, a renormalization factor was introduced to the calculated cross section.

In this coupled-channel analysis, only the deformation

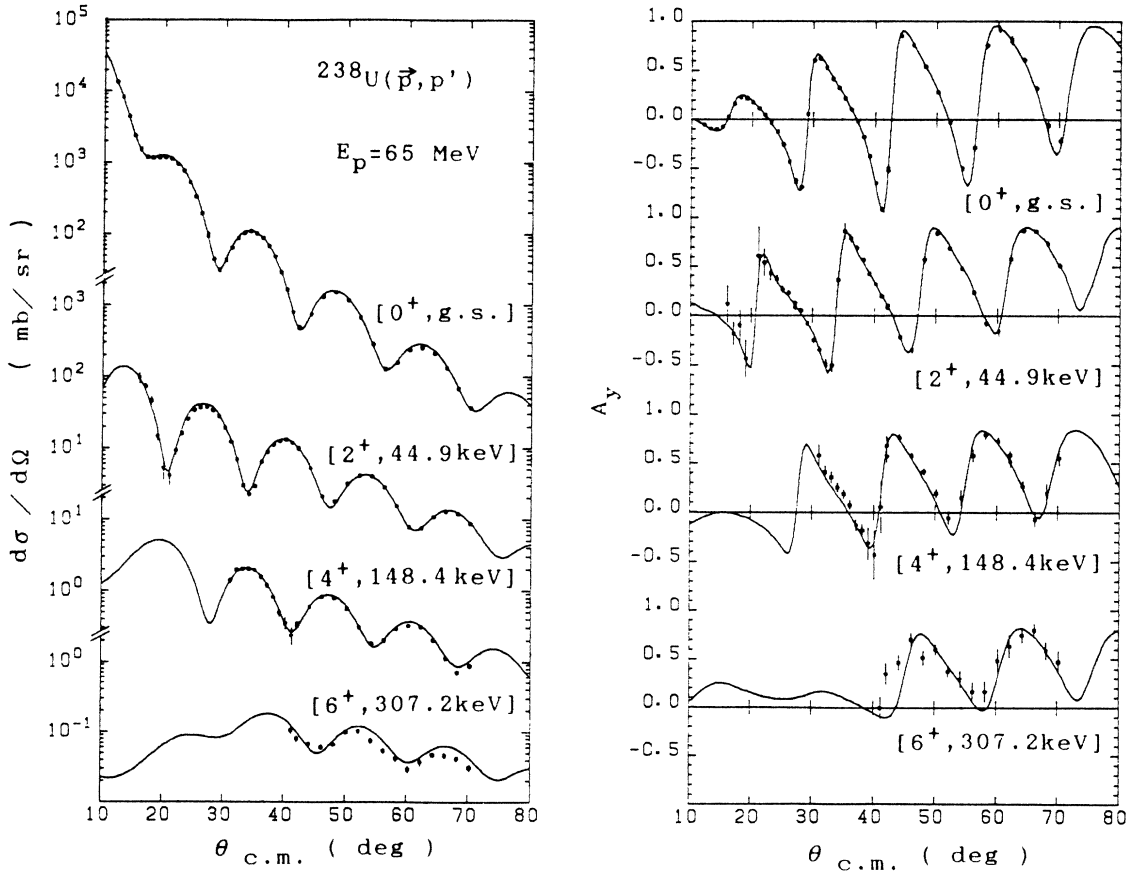

FIG. 4. Same as Fig. 3, except for ^{238}U.

TABLE I. (a) Best fit optical potential parameters of the coupled-channel analysis. Real central and spin-orbit parts, and renormalization factor. (b) Best fit optical potential parameters of the coupled-channel analysis. Volume and surface imaginary parts, and χ^2 per data point. (c) Best fit deformation parameters of the coupled-channel analysis. Real central and spin-orbit parts. (d) Best fit deformation parameters of the coupled-channel analysis. Volume and surface imaginary parts.

(a)

Nucleus	V_R (MeV)	r_R (fm)	a_R (fm)	V_{ls} (MeV)	r_{ls} (fm)	a_{ls} (fm)	Renormalization
^{232}Th	40.546	1.189	0.770	5.578	1.089	0.729	0.989
^{238}U	39.036	1.202	0.754	5.446	1.100	0.736	0.977

(b)

Nucleus	W_v (MeV)	r_{wv} (fm)	a_{wv} (fm)	W_s (MeV)	r_{ws} (fm)	a_{ws} (fm)	χ^2/N
^{232}Th	10.607	1.177	0.699	3.772	1.324	0.586	0.721
^{238}U	11.420	1.155	0.841	3.545	1.304	0.601	0.782

(c)

Nucleus	β_2^R	β_4^R	β_6^R	β_2^{ls}	β_4^{ls}	β_6^{ls}
^{232}Th	0.2135	0.0760	0.0041	0.2435	0.1010	0.0059
^{238}U	0.2308	0.0638	−0.0058	0.2646	0.0852	−0.0089

(d)

Nucleus	β_2^{wv}	β_4^{wv}	β_6^{wv}	β_2^{ws}	β_4^{ws}	β_6^{ws}
^{232}Th	0.2219	0.0857	0.0054	0.1854	0.0614	0.0041
^{238}U	0.2424	0.0671	−0.0064	0.2066	0.0544	−0.0043

parameters of the real central part of the DOP were searched. The deformation parameters of imaginary and spin-orbit part were not searched and were determined so that their multipole moments were equal to those of the real central part. Here, multipole moments of the DOP are defined as follows:

$$Q_\lambda^j = Ze \frac{\int f(r;r_j(\theta),a_j) Y_{\lambda 0}(\theta) r^{\lambda+2} dr\, d\Omega}{\int f(r;r_j(\theta),a_j) r^2 dr\, d\Omega} . \quad (5)$$

It is noted that, for the surface imaginary part and the spin-orbit part, the deformed Fermi form factor $f(r;r_j(\theta),a_j)$ in Eq. (2) was used instead of the potential itself. This procedure was the same as our previous work on Er and Yb isotopes.[2]

Recently, we have pointed out that the application of the above procedure to the imaginary and spin-orbit parts is not so straightforward and that the deformation parameters of each DOP part should be determined independent-

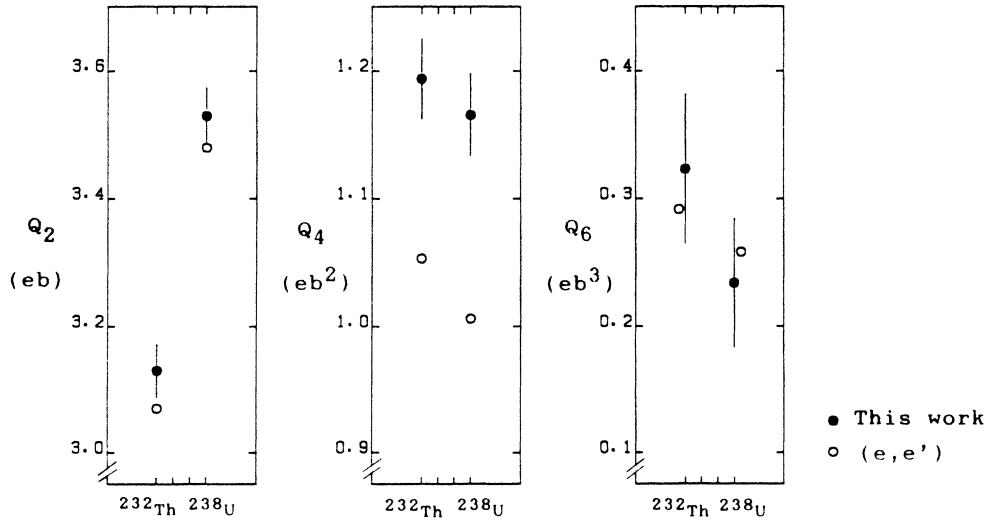

FIG. 5. The solid circles represent the multipole moments of the DOP derived from the present experiment. The open circles represent the charge multipole moments obtained from electron scattering. The data of ^{232}Th and ^{238}U are taken from Refs. 25 and 26, respectively.

ly.[3] In that case, precise data of the higher excited states as well as the forward angle data made it possible to search the deformation parameters independently. As mentioned in Sec. III A, however, the data at the forward angles have large uncertainties in the peak-sum extraction and the elastic peaks from the backing materials of the targets made it difficult to obtain precise data of higher excited states especially at forward angles. In the previous data of Hf and W isotopes, we have shown that the analysis in which β_λ's are independently searched agrees well in the multipole moments of the real central part with the other analysis in which β_λ's are related so as to reproduce the same multipole moments. For that reason, we have focused our discussion only on the multipole moments of the real central part and did not search the deformation parameters of other DOP parts independently.

The results of the coupled-channel analysis are shown in Figs. 3 and 4. Excellent fits have been obtained up to 6^+ states for both nuclei. The DOP parameters obtained in the analysis are listed in Table I.

In order to investigate the sensitivities of the data to the multipole moments, the total χ^2 value was calculated as a function of each multipole moment. In this paper the uncertainties in the multipole moments have been obtained from the values where the χ^2 value increases 10% from the minimum one. Extracted Q_2, Q_4, and Q_6 moments are shown in Fig. 5 with the uncertainties.

IV. DISCUSSION

A. Satchler's theorem and many-body effects

As discussed in our previous papers, Satchler's theorem plays an important role in understanding differences of multipole moments between different potentials.[2,10–14] For a folding model potential in which the underlying effective nucleon-nucleon interaction is assumed to depend only on the magnitude of the distance between the projectile nucleon and the nucleons in the target, the multipole moments of the potential are equal to those of the nuclear density as a result of Satchler's theorem. That is, if DOP $U(\mathbf{r})$ is given by

$$U(\mathbf{r})=\int \rho(\mathbf{r}_1)t(|\mathbf{r}-\mathbf{r}_1|)d\mathbf{r}_1 , \tag{6}$$

then

$$Q_\lambda^{\mathrm{DOP}}=Q_\lambda^{\mathrm{matter}} ,$$
$$Q_\lambda^{\mathrm{matter}}=\int \rho(\mathbf{r})r^\lambda Y_{\lambda 0}(\hat{\mathbf{r}})d\mathbf{r}\Big/\int \rho(\mathbf{r})d\mathbf{r} . \tag{7}$$

Therefore, if the multipole moments of the neutron density are equal to those of the proton density, multipole moments of the DOP should be equal to those of charge density in the limit where the DOP is equivalent to such a simple folding model potential, since the multipole moments of the charge density are equal to those of proton distribution. The many-body effects which are not included in the simple folding model described above will give rise to the difference of the multipole moments between the DOP and charge density.

In our previous works,[2,3] systematic 4–6% excess of the DOP quadrupole moment over that of the charge density was observed in the rare earth region, and was found to be quite consistent with the result of the folding model calculation based on the density dependent effective nucleon-nucleon interaction. As Brieva and Georgiev suggested,[14] however, other many-body effects such as nonlocality of the exchange term will also cause the difference in the multipole moments because such effects cannot be included in the simple folding model. Therefore, it is important and interesting to investigate such an effect in the study of the DOP multipole moments.

Since we will focus our discussion mainly on the differences of the multipole moments between the charge distri-

TABLE II. Multipole moments of the DOP and the charge densities.

Nucleus	Reaction	Q_2 (e b)	Q_4 (e b^2)	Q_6 (e b^3)
^{232}Th	(p,p′) at 65 MeV	3.132±0.042	1.190±0.033	0.348±0.07
	(e,e′) 50–320 MeV[a]	3.07	1.04	0.31
	(p,p′) at 35 MeV[b]	2.98 ±0.06	0.98 ±0.05	
	(p,p′) at 35 MeV[c]	2.82 ±0.04	0.98 ±0.04	0.30 ±0.04
	Coulomb excitation[d]	3.03 ±0.01	1.22 ±0.15	
	μ^- x ray[e]	3.03 ±0.02		
^{238}U	(p,p′) at 65 MeV	3.537±0.044	1.159±0.034	0.241±0.06
	(e,e′) 50–320 MeV[f]	3.48	0.99	0.27
	(p,p′) at 35 MeV[b]	3.30 ±0.06	0.81 ±0.06	
	(p,p′) at 35 MeV[c]	3.25 ±0.03	0.88 ±0.03	0.10 ±0.03
	Coulomb excitation[d]	3.51 ±0.02	0.83 ±0.22	
	μ^- x ray[g]	3.53 ±0.02	0.964±0.046	
	μ^- x ray[e]	3.51 ±0.01		

[a]Reference 26.
[b]Reference 4.
[c]Reference 5.
[d]Reference 27.
[e]Reference 29.
[f]Reference 25.
[g]Reference 28.

bution and the DOP, we introduce a quantity $\tilde{Q}_\lambda$ as follows:

$$\tilde{Q}_\lambda = (Q_\lambda^{\mathrm{DOP}} - Q_\lambda^{\mathrm{charge}})/Q_\lambda^{\mathrm{charge}} \times 100\ (\%)\ , \tag{8}$$

where we have used electron scattering data at the MIT Bates[25,26] Accelerator for Q_λ charge.

B. Extracted multipole moments of the DOP

In Table II we have summarized the extracted multipole moments of the present work with the data of inelastic proton scattering at another energy[4,5] and the charge multipole moments from electron scattering,[25,26] Coulomb excitation,[27] and muonic-atom experiments.[28,29] The DOP multipole moments are also plotted in Fig. 5 with the charge multipole moments of the electron scattering data at the MIT-Bates Accelerator. As shown in the figure, $\tilde{Q}_2$ values of this work are only 1.0—2.0 % for both the nuclei. These values are smaller, beyond the uncertainties, than the $\tilde{Q}_2$ of the rare earth nuclei, which have almost been explained by the effect of the density dependence. At 35 MeV, King *et al.* reported that $\tilde{Q}_2$ values of ^{232}Th and ^{238}U were also smaller ($\sim -5\%$) than those of ^{154}Sm and ^{176}Yb ($\sim -1\%$). There must be some other effects in actinide nuclei to compete with the effect of the density dependence.

In the case of Er and Yb isotopes, we have assumed that the Q_2 moments of the proton and neutron densities are equal because the Q_2 moment of the imaginary part of the DOP at 800 MeV (Ref. 6) was almost equal to that from electron scattering for ^{176}Yb. Since the impulse approximation gives a good description of the DOP in the energy region of several hundred MeV, the multipole moments of the DOP at 800 MeV are thought to be equal to those of matter distribution as a consequence of the Satchler's theorem. In the case of ^{232}Th and ^{238}U, however, we should take the difference of Q_2 moment between proton and neutron densities into consideration because of the lack of data at energies around several hundred MeV. The density-dependent Hartree-Fock (DDHF) calculation by Negele and Rinker[30] predicts that the neutron Q_2 moment is 3% larger than the proton Q_2 moment for ^{238}U. Since this trend of the neutron density makes the Q_2 moment of the folded potential still larger, the difference of the Q_2 moment between the neutron and the proton densities does not seem to explain the experimental fact that the $\tilde{Q}_2$ of the actinide nuclei is smaller than that of rare earth nuclei. Therefore, it is necessary to investigate other many-body effects which is not included in a simple folding model potential.

While the $\tilde{Q}_2$ is smaller than the prediction of density-dependent folding model, $\tilde{Q}_4$ is 14—18 % for both the nuclei. Although their signs are the same as caused by the effect of the density dependence, their magnitudes are too large to explain these values only by the density dependence, as is the case of Er and Yb isotopes. We will later discuss this in light of the result of the folding calculation.

C. Realistic folding model calculation

In order to explain the difference between Q_λ^{DOP} and $Q_\lambda^{\mathrm{charge}}$, we have carried out a realistic folding model calculation, following the formalism of Brieva and Rook.[31]

According to Brieva and Rook, the folded proton optical potential is written as

$$\begin{aligned} U_{\mathrm{p}}(\mathbf{r}_1,E_{\mathrm{in}}) = & \int \rho_{\mathrm{p}}(\mathbf{r}_2) T_D^{\mathrm{pp}}(s;\bar{\rho}_{\mathrm{p}}(\mathbf{R}),\tilde{E})d\mathbf{r}_2 + \int \rho_{\mathrm{n}}(\mathbf{r}_2) T_D^{\mathrm{pn}}(s;\bar{\rho}_{\mathrm{n}}(\mathbf{R}),\tilde{E})d\mathbf{r}_2 \\ & + \int \rho_{\mathrm{p}}(\mathbf{r}_1,\mathbf{r}_2) T_{\mathrm{ex}}^{\mathrm{pp}}(s;\bar{\rho}_{\mathrm{p}}(\mathbf{R}),\tilde{E}) j_0(ks)d\mathbf{r}_2 + \int \rho_{\mathrm{n}}(\mathbf{r}_1,\mathbf{r}_2) T_{\mathrm{ex}}^{\mathrm{pn}}(s;\bar{\rho}_{\mathrm{n}}(\mathbf{R}),\tilde{E}) j_0(ks)d\mathbf{r}_2\ , \end{aligned} \tag{9}$$

with

$$\begin{aligned} T_D^{\mathrm{pp}} &= (t^{01}+3t^{11})/4\ , \\ T_D^{\mathrm{pn}} &= (t^{01}+3t^{11}+3t^{10}+t^{00})/8\ , \\ T_{\mathrm{ex}}^{\mathrm{pp}} &= (t^{01}-3t^{11})/4\ , \\ T_{\mathrm{ex}}^{\mathrm{pn}} &= (t^{01}-3t^{11}+3t^{10}-t^{00})/8\ , \end{aligned} \tag{10}$$

$$\begin{aligned} \bar{\rho}_{\mathrm{p}}(\mathbf{R}) &= \rho_{\mathrm{p}}(\mathbf{R})\ , \\ \bar{\rho}_{\mathrm{n}}(\mathbf{R}) &= [\rho_{\mathrm{p}}(\mathbf{R})+\rho_{\mathrm{n}}(\mathbf{R})]/2\ , \\ \mathbf{R} &= (\mathbf{r}_1+\mathbf{r}_2)/2\ , \end{aligned} \tag{11}$$

where E_{in} is the incident energy of the projectile proton, $s = |\mathbf{r}_1-\mathbf{r}_2|$, and $j_0(r)$ is a spherical Bessel function of order zero. $\tilde{E}$ is the effective local energy which includes the effect of the Coulomb potential through the energy dependence of the effective interaction (so-called Coulomb correction):[31,32]

$$\tilde{E}(\mathbf{r}) = E_{\mathrm{in}} - V_{\mathrm{Coul}}(\mathbf{r})\ . \tag{12}$$

$\rho_{\mathrm{p}}(\mathbf{r})$ and $\rho_{\mathrm{n}}(\mathbf{r})$ represent the proton and neutron distributions, respectively. $t^{ST}(r;\rho,E)$ is the nucleon-nucleon effective interaction in states of spin S and isospin T. The local momentum k of the incident proton is defined as

$$k(\mathbf{r}) = \{2m[E_{\mathrm{in}} - V_{\mathrm{Coul}}(\mathbf{r}) - \mathrm{Re}U_{\mathrm{p}}(\mathbf{r},E_{\mathrm{in}})]\}^{1/2}\ . \tag{13}$$

U_{p} and k were calculated self-consistently by iteration. For the mixed density matrix $\rho_{\mathrm{p(n)}}(\mathbf{r}_1,\mathbf{r}_2)$ in the exchange term, the approximation of Negele and Vautherin[32] was used:

$$\rho_{\mathrm{p(n)}}(\mathbf{r}_1,\mathbf{r}_2) = \rho_{\mathrm{p(n)}}(\mathbf{R}) \frac{3}{(sk_F^{\mathrm{p(n)}})^3} [\sin(sk_F^{\mathrm{p(n)}}) - sk_F^{\mathrm{p(n)}} \cos(sk_F^{\mathrm{p(n)}})]\ , \tag{14}$$

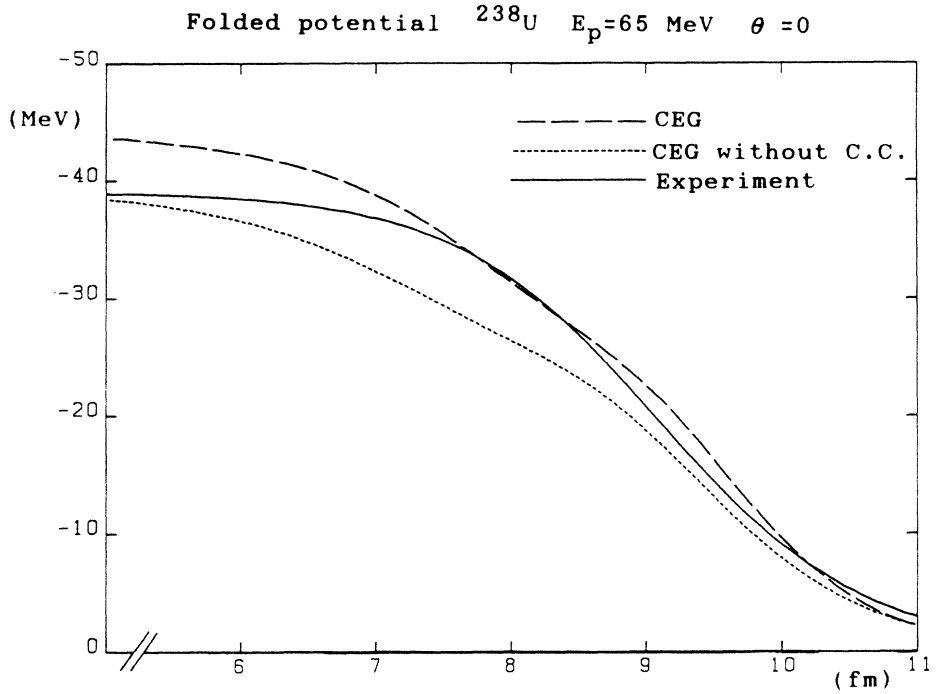

FIG. 6. Radial shape of the folded potential along the symmetry axis ($\theta=0$). The dashed curve represents the folded potential using an effective interaction CEG. The details of the folding procedure are described in the text. The dotted curve is the same as the dashed curve, except that the Coulomb correction is not included in the folding calculation. The solid curve represents the phenomenological deformed Woods-Saxon potential obtained from the coupled-channel analysis of this experiment.

where

$$k_F^{p(n)}=[\tfrac{3}{2}\pi^2\rho_{p(n)}(\mathbf{R})]^{1/3} .$$

In this folding calculation, $\rho_p(\mathbf{r})$ and $\rho_n(\mathbf{r})$ were assumed to be the deformed Woods-Saxon shape and their parameters were derived from the charge distribution with the same procedure as our previous works. As for the t^{ST}, we have used the density- and energy-dependent effective interaction CEG (complex effective Gaussian interaction) by Nagata *et al.*,[34,35] which gives a parameter-free description of the elastic scattering at energies lower than 100 MeV.

The radial shape of the folded potential is shown in Fig. 6, with the phenomenological deformed Woods-Saxon potential obtained in the coupled-channel analysis. Considering the fact that the folded potential has no adjustable parameters, the agreement is remarkably good.

According to Satchler's theorem, the density dependence of the effective interaction, the exchange effect, and the Coulomb correction will cause the difference between $Q_\lambda^{\text{matter}}$ and Q_λ^{DOP} in this formalism.

1. Quadrupole moments

The results of the folding calculation are shown in Table III and Fig. 7 (represented by the solid circles). As can be noticed in the figure, the $\tilde{Q}_2$ values of the present folding method exhibit an excellent agreement with those obtained from the experiment (represented by the squares with error bars in Fig. 7). Triangles and crosses in Fig. 7 represent the $\tilde{Q}_2$ values calculated with our previous method[2] in which the effective interaction $M3Y$ (Ref. 36) and exchange term proposed by Kobos *et al.*[37] are used and the density-dependent factors are those of Green[38] (crosses) and of Jeukenne, Lejeune, and Mahaux[33] (JLM) (triangles), respectively. The $\tilde{Q}_2$ values calculated with the previous method are much larger than those from the present experiment. In the previous folding method, the exchange effect was treated less sufficiently than the present method, and the Coulomb correction could not be included since the effective interaction $M3Y$ has no explicit energy dependence.

In order to investigate the contribution from the Coulomb correction, we have performed another calculation in which $V_{\text{Coul}}(r)$ in Eq. (12) is set to zero (represented by the open circles in Fig. 7). The $\tilde{Q}_2$ values of this calculation are considerably larger than the full calculation. Therefore, the effect of the Coulomb correction is the opposite of the effect of the density dependence and reduces the Q_2 moment of the DOP. The Coulomb correction plays an important role in the DOP of the actinide nuclei. A simple explanation for this effect is as follows: Since the Coulomb force has long range, the Coulomb potential (not the charge distribution) is less deformed than the DOP (see Fig. 8). The local energy $\tilde{E}$ is smaller near the equator (point A in Fig. 8) than near the pole (point B). Then, the Coulomb correction makes the folded potential deeper near the equator than near the pole; that is, the deformation of the DOP is reduced.

The differences between the triangles ($M3Y$ with the density dependence of JLM and the exchange term of Kobos *et al.*) and the open circles (the present folding calculation without the Coulomb correction) may be attributed to the difference in the exchange term since the density

dependence of the CEG and that of JLM are not so different. However, it is not so easy to explain the contribution from the exchange effect because of its complication.

2. *Hexadecapole moments*

The calculated hexadecapole moments are also shown in Fig. 7. In contrast with the Q_2 moments, Q_4^{expt} is about 10% larger than Q_4^{calc} using CEG, which gives the best results in the Q_2 moment. It should be noted that the error bar of $\tilde{Q}_4^{\text{expt}}$ in Fig. 7 includes only uncertainty in the Q_4 moment of the DOP. As can be noticed in Eq. (8), however, uncertainty in $\tilde{Q}_4^{\text{expt}}$ must include uncertainty in Q_4^{charge}. The electron scattering data at the MIT-Bates Accelerator were analyzed with two different charge distributions.[25,26] One is the conventional deformed Fermi distribution, called SDF (single deformed Fermi distribution), and the other is called MDF (multiple deformed Fermi distribution), which allows different deformation parameters for different multipoles. In this work, the $Q_\lambda^{\text{charge}}$ values are taken from the results with the SDF because of the simplicity in the folding calculation. The differences in Q_2^{charge} values between the SDF and the MDF are less than 1% and are negligible for our discussion, while the differences in Q_4^{charge} amount to nearly 10%. Therefore, the Q_4^{charge} values are thought to have at

TABLE III. Results of the folding model calculation.

Nucleus		Q_2 (e b)	Q_4 (e b^2)
^{232}Th	(p,p′) at 65 MeV	3.132±0.042	1.190±0.033
	matter distribution[a]	3.07	1.04
	folded (CEG)[b]	3.101	1.092
	folded (CEG without Coulomb correction)[c]	3.153	1.120
	folded ($M3Y$ with JLM density dependence)[d]	3.184	1.150
	folded ($M3Y$ with Green's density dependence)[d]	3.221	1.185
^{238}U	(p,p′) at 65 MeV	3.537±0.044	1.159±0.034
	matter distribution[e]	3.48	0.99
	folded (CEG)[b]	3.518	1.036
	folded (CEG without Coulomb correction)[c]	3.573	1.061
	folded ($M3Y$ with JLM density dependence)[d]	3.611	1.091
	folded ($M3Y$ with Green's density dependence)[d]	3.653	1.136
^{166}Er	(p,p′) at 65 MeV[f]	2.511±0.032	0.252±0.020
	matter distribution[e]	2.41	0.294
	folded (CEG)[b]	2.458	0.308
	folded (CEG without Coulomb correction)[c]	2.490	0.313
	folded ($M3Y$ with JLM density dependence)[d]	2.524	0.320
	folded ($M3Y$ with Green's density dependence)[d]	2.562	0.330
^{176}Yb	(p,p′) at 65 MeV[f]	2.436±0.032	−0.071±0.020
	matter distribution[e]	2.30	−0.013
	folded (CEG)[b]	2.347	−0.020
	folded (CEG without Coulomb correction)[c]	2.374	−0.023
	folded ($M3Y$ with JLM density dependence)[d]	2.403	−0.026
	folded ($M3Y$ with Green's density dependence)[d]	2.437	−0.030

[a]Reference 26.
[b]Present folding procedure using effective interaction CEG.
[c]Present folding procedure, but the Coulomb correction was not included.
[d]Folding procedure using effective interaction $M3Y$. The details of the folding procedure are described in Ref. 2.
[e]Reference 25.
[f]Reference 2.

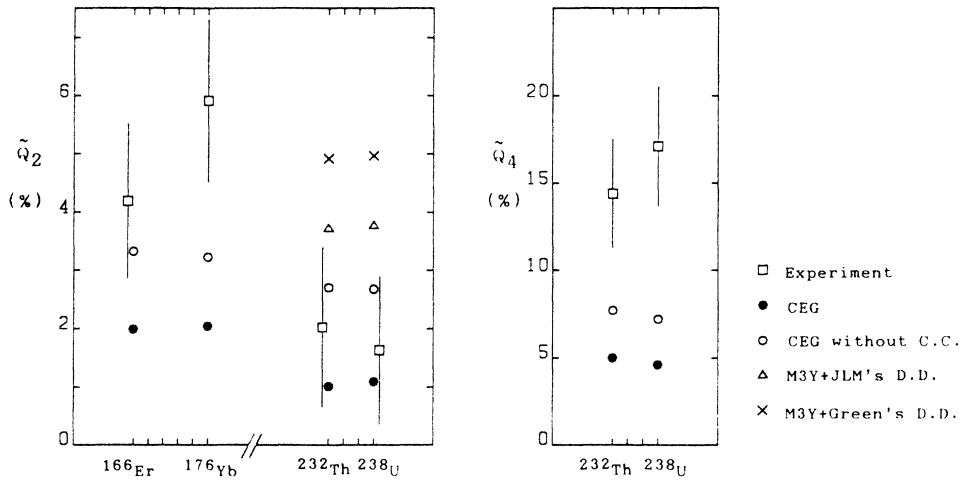

FIG. 7. The open squares are the experimental results obtained from the inelastic scattering of protons at 65 MeV. The data of ^{166}Er and ^{176}Yb are taken from Ref. 2. The solid circles are the results of the folding calculation using an effective interaction CEG. The open circles are the same as the solid circles, except that the Coulomb correction is not included in the folding calculation. The triangles are the results using modified $M3Y$ interaction, whose density dependence is that of JLM. The crosses are the same as the triangles, except that the density dependence used is that of Green.

least 10% uncertainties owing to the form factor used in their analysis.

However, there is another possibility, namely that the discrepancy may arise from the different density distributions between protons and neutrons. The higher order multipole moments are thought to be sensitive to the details of nuclear structure, such as the difference between proton and neutron distribution. We have already reported that the hexadecapole moments of Er and Yb isotopes cannot be reproduced by folding model calculation. More recently, Lay *et al.* have reported[8] that the hexadecapole moment of ^{176}Yb at 134 MeV is also very close to the value at 65 MeV. The DDHF calculations by Negele and Rinker[30] predict a systematic 10—15 % excess of the hexadecapole moment of the neutron density over those of proton for the nuclei which have a large positive hexadecapole moment. At the present stage, it is difficult to draw a definite conclusion from the differences between $Q_4^{\rm calc}$ and $Q_4^{\rm expt}$.

3. *Comparison with Q_2 moments of rare earth nuclei*

The present folding model calculation has also been performed for the rare earth nuclei for comparison. The results are shown in Fig. 7. The $\tilde{Q}_2^{\rm calc}$ values are about 2%, which is smaller than the $\tilde{Q}_2^{\rm expt}$ values by 2—3 %. In the case of ^{176}Yb, the difference of $Q_2^{\rm charge}$ between the MDF and SDF amounts to 2%. If we take the $Q_2^{\rm charge}$ from the MDF, the $\tilde{Q}_2^{\rm expt}$ of ^{176}Yb becomes closer to the $\tilde{Q}_2^{\rm calc}$. It is noted that the Coulomb correction in the folding calculation yields considerable difference of $\tilde{Q}_2$ between actinide and rare earth nuclei because of the difference in atomic number. The effect of the Coulomb correction improves the discrepancy of the $\tilde{Q}_2$ between the rare-earth and the actinide nuclei, though the improvement is not complete. Therefore, the Coulomb correction is thought to be an important source of the difference of $\tilde{Q}_2$ between the actinide and the rare earth nuclei. Residual disagreement between the $Q_2^{\rm expt}$ and the $Q_2^{\rm calc}$ in the rare earth nuclei suggests that further improvements of the effective interaction and the folding procedure are necessary.

V. SUMMARY AND CONCLUSION

We have measured the differential cross sections and the analyzing powers of elastic and inelastic scattering of 65 MeV polarized protons from ^{232}Th and ^{238}U. We have analyzed for the members of the ground state rotational band up to $J^\pi = 6^+$ state using the coupled-channel calculation assuming the axially symmetric rotor model. Very excellent fits have been obtained up to the 6^+ state.

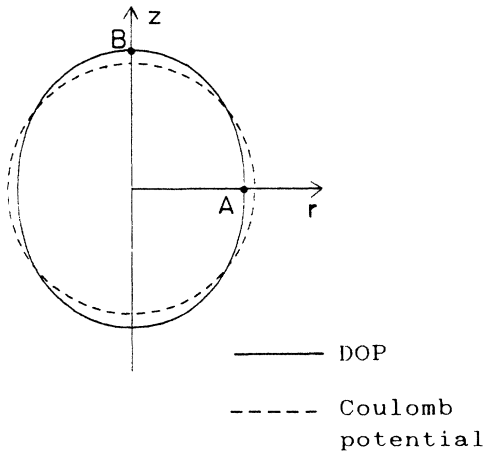

FIG. 8. The solid curve represents the equipotential surface of the DOP calculated without the Coulomb correction. The dashed curve represents the equipotential surface of the Coulomb potential. The local energy, $\tilde{E} = E_{\rm in} - V_{\rm Coul}$, is larger at point B than at point A. If the Coulomb correction is taken into account by the local-energy approximation, the DOP becomes deeper at point A than at point B. Then, the deformation of the DOP becomes smaller.

The multipole moments of $\lambda=2$, 4, and 6 of the DOP have been compared with those of the charge densities. The quadrupole moments of the DOP are only 1—2% larger than those of the charge densities. These values cannot be explained only by the effect of the density dependence of the effective interaction. In order to investigate contributions of other corrections to the simple folding model, we have performed a more realistic folding calculation, using a density- and energy-dependent effective interaction CEG. This calculation successfully reproduces the quadrupole moments of ^{232}Th and ^{238}U. Rigorous treatment of the exchange effect and the inclusion of the Coulomb correction have been found to be necessary for reproducing the experimental values. A large part of the discrepancy between the actinide and rare earth nuclei is also improved by including the Coulomb correction, although the agreement in the rare earth nuclei is not as good as in the actinide nuclei. Therefore, the Coulomb correction plays an important role in these nuclei.

The trends of the hexadecapole moments of the DOP and of the charge densities are very similar to the case of the rare earth nuclei, but the hexadecapole moments of the DOP are 14—18% larger than the charge hexadecapole moments. Two possibilities have been discussed for the difference between the charge and the DOP hexadecapole moment. One is significant uncertainties in extracting the charge moment. The other is the difference of the hexadecapole moment between proton and neutron densities. Further systematic research with electrons and protons is necessary for the understanding of the hexadecapole moments, and it will offer new knowledge of the effective nucleon-nucleon interaction and the nuclear structure of the deformed nuclei.

ACKNOWLEDGMENTS

The authors wish to express their thanks to Professor H. Ikegami, Professor S. Morinobu, Dr. M. Fujiwara, and Dr. Y. Fujita for their advice in the operation of the spectrograph RAIDEN and its focal counter system, and to Dr. N. Matsuoka for the operation of the polarized ion source. We are indebted to Professor I. Fjiwara at the Institute of Atomic Energy, Kyoto University, for his advice and cooperation in the target preparation. Sincere thanks are also expressed to Professor S. Nagata at Miyazaki University for the usage of his effective interaction and for his advice and discussion in calculating the folded potentials. The data reduction, coupled-channel analysis, and folding model calculations were performed with the computers FACOM M-180-2AD and FACOM M-200 at the Research Center for Nuclear Physics, Osaka University, and FACOM M-340 at the Department of Physics, Kyoto University. The experiment was performed at the Research Center for Nuclear Physics, Osaka University, under Program No. 18A25 and was supported in part by a Grant-in-Aid for Scientific Research, No. 60420007, of the Japan Ministry of Education, Science and Culture.

*Present address: Institute of Physical and Chemical Research, Wako, Saitama 351, Japan.

[1]F. Ohtani, H. Sakaguchi, M. Nakamura, T. Noro, H. Sakamoto, H. Ogawa, T. Ichihara, M. Yosoi, and S. Kobayashi, Phys. Rev. C **28**, 120 (1983).

[2]T. Ichihara, H. Sakaguchi, M. Nakamura, T. Noro, F. Ohtani, H. Sakamoto, H. Ogawa, M. Yosoi, M. Ieiri, N. Isshiki, and S. Kobayashi, Phys. Rev. C **29**, 1228 (1984).

[3]H. Ogawa, H. Sakaguchi, M. Nakamura, T. Noro, H. Sakamoto, T. Ichihara, M. Yosoi, M. Ieiri, N. Isshiki, Y. Takeuchi, and S. Kobayashi, Phys. Rev. C **33**, 834 (1986).

[4]C. H. King, J. E. Finck, G. M. Crawley, J. A. Nolen, Jr., R. M. Ronningen, Phys. Rev. C **20**, 2084 (1979).

[5]R. M. Ronningen, R. C. Melin, J. A. Nolen, Jr., G. M. Crawley, and C. E. Bemis, Jr., Phys. Rev. Lett. **31**, 635 (1981).

[6]M. L. Barlett, J. A. McGill, L. Ray, M. M. Barlett, G. W. Hoffmann, N. M. Hintz, G. S. Kyle, M. A. Franey, and G. Blanpied, Phys. Rev. C **22**, 1168 (1980).

[7]R. M. Ronningen, G. M. Crawley, N. Anantaraman, S. M. Banks, B. M. Spicer, G. G. Shute, V. C. Officer, J. M. R. Wastell, D. W. Devins, and D. L. Friesel, Phys. Rev. C **28**, 123 (1983).

[8]B. G. Lay, S. M. Banks, B. M. Spicer, G. G. Shute, V. C. Officer, R. M. Ronningen, G. M. Crawley, N. Anantaraman, and R. P. DeVito, Phys. Rev. C **32**, 440 (1985).

[9]H. Sakaguchi, M. Nakamura, K. Hatanaka, A. Goto, T. Noro, F. Ohtani, H. Sakamoto, H. Ogawa, and S. Kobayashi, Phys. Rev. C **26**, 944 (1982).

[10]G. R. Satchler, J. Math. Phys. **13**, 1118 (1972).

[11]R. S. Mackintosh, Nucl. Phys. **A266**, 379 (1976).

[12]J. K. Hamilton and R. S. Mackintosh, J. Phys. G **4**, 557 (1978).

[13]R. S. Mackintosh, J. Phys. G **4**, 547 (1978).

[14]F. A. Brieva and B. Z. Georgiev, Nucl. Phys. **A308**, 27 (1978).

[15]F. A. Brieva and J. R. Rook, Nucl. Phys. **A297**, 206 (1978).

[16]H. Ikegami, S. Morinobu, I. Katayama, M. Fujiwara, and S. Yamabe, Nucl. Instrum. Methods **175**, 335 (1980).

[17]K. Imai, N. Tamura, and K. Nishimura, Research Center for Nuclear Physics Annual Report, 1976, p. 76 (unpublished).

[18]T. Ichihara, H. Sakaguchi, K. Hatanaka, M. Fujiwara, and K. Hosono, Research Center for Nuclear Physics Annual Report, 1981, p. 194 (unpublished).

[19]J. E. Evans, R. W. Lougheed, M. S. Coops, R. W. Hoff, and E. K. Hulet, Nucl. Instrum. Methods **102**, 386 (1972).

[20]D. C. Aumann and G. Muellen, Nucl. Instrum. Methods **115**, 75 (1974).

[21]Y. Fujita, K. Nagayama, M. Fujiwara, S. Morinobu, T. Yamazaki, and H. Ikegami, Nucl. Instrum. Methods **196**, 249 (1982).

[22]H. P. Blok, J. C. Delange, and J. W. Schotman, Nucl. Instrum. Methods **128**, 545 (1975).

[23]J. Raynal, code ECIS79, Saclay (unpublished).

[24]J. Raynal, International Atomic Agency Report No. IAEA-5MR-818, 1972, p. 75 (unpublished).

[25]C. W. Creswell, Ph.D. thesis, MIT, 1977 (unpublished).

[26]A. S. Hirsch, Ph.D. thesis, MIT, 1977 (unpublished).

[27]C. E. Bemis, Jr. *et al.*, Phys. Rev. C **8**, 1466 (1973).

[28]J. D. Zumbro, E. B. Shera, Y. Tanaka, C. E. Bemis, Jr., R. A. Naumann, M. V. Hoehn, W. Reuter, and R. M. Steffen, Phys. Rev. Lett. **53**, 1888 (1984).

[29]D. A. Close, J. J. Malanify, and J. P. Davidson, Phys. Rev. C **17**, 1433 (1978).
[30]J. W. Negele and G. Rinker, Phys. Rev. C **15**, 1499 (1979).
[31]F. A. Brieva and J. R. Rook, Nucl. Phys. **A291**, 317 (1977).
[32]J. P. Jeukenne, A. Lejeune, and C. Mahaux, Phys. Rev. C **16**, 80 (1977).
[33]J. W. Negele and D. Vautherin, Phys. Rev. C **5**, 1472 (1972).
[34]N. Yamaguchi, S. Nagata, T. Matsuda, Prog. Theor. Phys. **70**, 456 (1983).
[35]S. Nagata, M. Kamimura, and N. Yamaguchi, Prog. Theor. Phys. **73**, 512 (1985).
[36]G. Bertsch, J. Borysowicz, H. McManus, and W. G. Love, Nucl. Phys. **A284**, 399 (1977).
[37]A. M. Kobos, B. A. Brown, P. E. Hodgson, G. R. Satchler, and A. Budzanowski, Nucl. Phys. **A384**, 65 (1982).
[38]A. M. Green, Phys. Lett. **24B**, 384 (1967).